2012

I=2 pi pi S-wave scattering phase shift from lattice QCD

S. R. Beane

S. R. Beane

E. Chang

W. Detmold
William & Mary

K. Orginos
William & Mary, kostas@wm.edu

PHYSICAL REVIEW D **85,** 034505 (2012)

$I = 2$ $\pi\pi$ S-wave scattering phase shift from lattice QCD

S. R. Beane,[1,2] E. Chang,[3] W. Detmold,[4,5] H. W. Lin,[6] T. C. Luu,[7] K. Orginos,[4,5] A. Parreño,[3] M. J. Savage,[6] A. Torok,[8] and A. Walker-Loud[9]

(NPLQCD Collaboration)

[1]*Albert Einstein Zentrum für Fundamentale Physik, Institut für Theoretische Physik, Sidlerstrasse 5, CH-3012 Bern, Switzerland*
[2]*Department of Physics, University of New Hampshire, Durham, New Hampshire 03824-3568, USA*
[3]*Departament d'Estructura i Constituents de la Matèria. Institut de Ciències del Cosmos (ICC), Universitat de Barcelona, Martí i Franquès 1, E08028-Spain*
[4]*Department of Physics, College of William and Mary, Williamsburg, Virginia 23187-8795, USA*
[5]*Jefferson Laboratory, 12000 Jefferson Avenue, Newport News, Virginia 23606, USA*
[6]*Department of Physics, University of Washington, Box 351560, Seattle, Washington 98195, USA*
[7]*N Division, Lawrence Livermore National Laboratory, Livermore, California 94551, USA*
[8]*Department of Physics, Indiana University, Bloomington, Indiana 47405, USA*
[9]*Lawrence Berkeley National Laboratory, Berkeley, California 94720, USA*
(Received 20 September 2011; published 16 February 2012)

The $\pi^+\pi^+$ s-wave scattering phase shift is determined below the inelastic threshold using lattice QCD. Calculations were performed at a pion mass of $m_\pi \sim 390$ MeV with an anisotropic $n_f = 2 + 1$ clover fermion discretization in four lattice volumes, with spatial extent $L \sim 2.0$, 2.5, 3.0 and 3.9 fm, and with a lattice spacing of $b_s \sim 0.123$ fm in the spatial direction and $b_t \sim b_s/3.5$ in the time direction. The phase shift is determined from the energy eigenvalues of $\pi^+\pi^+$ systems with both zero and nonzero total momentum in the lattice volume using Lüscher's method. Our calculations are precise enough to allow for a determination of the threshold scattering parameters, the scattering length a, the effective range r, and the shape parameter P, in this channel and to examine the prediction of two-flavor chiral perturbation theory: $m_\pi^2 ar = 3 + \mathcal{O}(m_\pi^2/\Lambda_\chi^2)$. Chiral perturbation theory is used, with the lattice QCD results as input, to predict the scattering phase shift (and threshold parameters) at the physical pion mass. Our results are consistent with determinations from the Roy equations and with the existing experimental phase shift data.

DOI: 10.1103/PhysRevD.85.034505 PACS numbers: 12.38.Gc

I. INTRODUCTION

Pion-pion ($\pi\pi$) scattering at low energies is the theoretically simplest and best-understood hadronic scattering process. Its simplicity and tractability follow from the pseudo-Goldstone boson nature of the pion, a consequence of the spontaneously broken chiral symmetry of QCD, which implies powerful constraints on its low-momentum interactions. The amplitudes for $\pi\pi$ scattering are uniquely predicted at leading order (LO) in chiral perturbation theory (χPT) [1]. Subleading orders in the chiral expansion give rise to perturbatively-small deviations from the LO determinations (for small pion masses), and contain both calculable nonanalytic contributions and analytic terms with low-energy constants (LEC's) that cannot be determined by chiral symmetry alone [2–4]. Fortunately, lattice QCD calculations are reaching a level of precision where statistically significant values of the LEC's in the $I = 2$ ($\pi^+\pi^+$) channel are being calculated. Once the LEC's are obtained using unphysical lattice pion masses, χPT can be used to predict the phase shift at the physical pion mass to relatively high precision and with quantified uncertainties. The current capability of lattice QCD—in conjunction with χPT—to calculate $\pi\pi$ scattering parameters very accurately is important theoretically because Roy-equation [5–7] determinations of $\pi\pi$ scattering parameters, which use dispersion theory to relate scattering data at high energies to the scattering amplitude near threshold, have also reached a remarkable level of precision [8–10], and the results of the two methods can now be compared and contrasted.

There have been independent lattice QCD determinations of the $\pi^+\pi^+$ scattering length; with three flavors ($n_f = 2 + 1$) of light quarks using domain-wall valence quarks on asqtad-improved staggered sea quarks [11,12], and with two flavors ($n_f = 2$) of light quarks using twisted-mass quarks [13] and improved Wilson quarks [14–17]. These determinations are in agreement with the Roy equation values. The first calculation of the $\pi^+\pi^+$ scattering phase shift was carried out by the CP-PACS Collaboration, who exploited the finite-volume strategy to study s-wave scattering with $n_f = 2$ improved Wilson fermions [14,15] at pion masses in the range $m_\pi \simeq$ 500–1100 MeV. The amplitudes obtained from the Lattice QCD calculations were extrapolated to the physical mass using a polynomial dependence upon the pion mass, instead of using the known pion-mass dependence of the amplitude based upon the symmetries of QCD encapsulated in χPT. In a recent paper, the Hadron Spectrum Collaboration (HSC) studied the s wave $\pi^+\pi^+$ phase shift with pion masses in the range $m_\pi \simeq 390$–520 MeV [18]. Further, they have provided the first lattice QCD calculation of the $\pi^+\pi^+$ phase shift in the d-wave ($l = 2$) [18].

In this work, which is a continuation of our high statistics lattice QCD explorations [19–23], we determine the $\pi^+\pi^+$ scattering amplitude below the inelastic threshold. Calculations are performed with four ensembles of $n_f = 2+1$ anisotropic clover gauge-field configurations at a single pion mass of $m_\pi \sim 390$ MeV with a spatial lattice spacing of $b_s \sim 0.123$ fm, an anisotropy of $\xi \sim 3.5$, and with cubic spatial volumes of extent $L \sim 2.0$, 2.5, 3.0 and 3.9 fm. Predictions are made for a number of threshold parameters which encode the leading momentum-dependence of the scattering amplitude, and dictate the scattering length, effective range and shape parameters in the effective range expansion (ERE) of the inverse scattering amplitude. The lattice QCD predictions are found to be in agreement with the Roy-equation determinations of the threshold parameters and phase shift, and with the available experimental data. Beyond the threshold region, the LEC's that contribute to the two-flavor chiral expansion of the scattering amplitude are determined, allowing for a prediction of the phase shift at the physical pion mass to be performed at next-to-leading order (NLO). The predicted phase shift is in agreement with the experimental data.

The Maiani-Testa theorem demonstrates that S-matrix elements cannot be determined from stochastic lattice calculations of n-point Green's functions at infinite volume, except at kinematic thresholds [24]. Lüscher showed that by computing the energy levels of two-particle states in the finite-volume lattice, the $2 \to 2$ scattering amplitude can be recovered [25–34]. These energy levels are found to deviate from those of two noninteracting particles by an amount that depends on the scattering amplitude (evaluated at that energy) and varies inversely with the lattice spatial volume in asymptotically large volumes. In this paper, Lüscher's method is used to extract the phase shift from the lattice-determined energy levels.

This paper is organized as follows. In Sec. II, we provide some details of the lattice calculations: we discuss the anisotropic clover lattices that are used and the determination of the anisotropy parameter. Sec. III gives a summary of the eigenvalue equation which is relevant to extracting phase shifts from lattice-measured energy levels, in the center-of-mass (CoM) system and in boosted (lattice = laboratory) systems. The results of the lattice QCD calculations are presented in Sec. IV and relevant fits that are used to determine the effective range parameters, up to and including the shape parameter, are discussed. Sec. V includes a summary of the relevant χPT formulas, the chiral fits to the lattice data, and the prediction for the $\pi^+\pi^+$ phase shift up to the inelastic threshold at the physical pion mass. Finally, a summary of our predictions and a discussion of the systematic uncertainties are given in Sec. VI.

II. DETAILS OF THE LATTICE QCD CALCULATIONS

A. Anisotropic clover lattices

Anisotropic gauge-field configurations have proven useful for the study of hadronic spectroscopy [35–38], and, as the calculations required for studying multihadron systems rely heavily on spectroscopy, we have put considerable effort into calculations using ensembles of gauge fields with clover-improved Wilson fermion actions with anisotropic lattice spacing that have been generated by the HSC. In particular, the $n_f = 2+1$ flavor anisotropic clover Wilson action [39,40] with stout-link smearing [41] of the spatial gauge fields in the fermion action with a smearing weight of $\rho = 0.14$ and $n_\rho = 2$ has been used. The gauge fields entering the fermion action are not smeared in the time direction, thus preserving the ultralocality of the action in the time direction. Further, a tree-level tadpole-improved Symanzik gauge action without a 1×2 rectangle in the time direction is used.

The present calculations are performed on four ensembles of gauge-field configurations with $L^3 \times T$ of $16^3 \times 128$, $20^3 \times 128$, $24^3 \times 128$ and $32^3 \times 256$ lattice sites, with a renormalized anisotropy $\xi = b_s/b_t$ where b_s and b_t are the spatial and temporal lattice spacings, respectively. The spatial lattice spacing of each ensemble is $b_s = 0.1227 \pm 0.0008$ fm [37] giving spatial lattice extents of $L \sim 2.0$, 2.5, 3.0 and 3.9 fm, respectively. The same input light-quark mass parameters, $b_t m_l = -0.0840$ and $b_t m_s = -0.0743$, are used in the production of each ensemble, giving a pion mass of $m_\pi \sim 390$ MeV. The relevant quantities to assign to each ensemble that determine the impact of the finite lattice volume and temporal extent are $m_\pi L$ and $m_\pi T$, which are given in Table I. In addition, we tabulate the pion masses on the four

TABLE I. Results from the lattice QCD calculations in the four lattice volumes. t.l.u denotes temporal lattice units.

$L^3 \times T$	$16^3 \times 128$	$20^3 \times 128$	$24^3 \times 128$	$32^3 \times 256$
L(fm)	$\sim$2.0	$\sim$2.5	$\sim$3.0	$\sim$3.9
$m_\pi L$	3.888(20)(01)	4.8552(84)(35)	5.799(16)(04)	7.7347(74)(91)
$m_\pi T$	8.89(16)(01)	8.878(54)(22)	8.836(85)(02)	17.679(59)(73)
m_π (t.l.u.)	0.069 43(36)(0)	0.069 36(12)(0)	0.069 03(19)(0)	0.069 060(66)(81)

lattice volumes. As discussed in detail in Ref. [22], exponential finite-volume corrections to the pion masses are negligible for these volumes, a necessary condition for the application of Lüscher's finite-volume method for obtaining phase shifts. Additionally, the predicted exponential finite-volume corrections to $\pi\pi$ scattering near threshold are expected to be negligible [42]. Multiple light-quark propagators were calculated on each configuration in the four ensembles. The source locations were chosen randomly in an effort to minimize correlations among propagators.

B. Determination of the anisotropy parameter, ξ

In the continuum and in infinite volume, the energy-momentum relation for the pion is that of special relativity, $E^2 = m_\pi^2 + |\mathbf{p}|^2$. In lattice QCD calculations, this relation is more complicated due to the finite lattice spacing (including the violation of Lorentz invariance) and the finite volume, resulting in E^2 being a nontrivial function of $\mathbf{p}$, which has a polynomial expansion at small momentum. Retaining the leading terms in the energy-momentum relation, including the lattice anisotropy ξ, the energy and mass in temporal lattice units, and the momentum in spatial lattice units (s.l.u) are related by

$$(b_t E_\pi(|\mathbf{n}|))^2 = (b_t m_\pi)^2 + \frac{1}{\xi^2}\left(\frac{2\pi b_s}{L}\right)^2 \mathbf{n}^2. \tag{1}$$

The lattice QCD calculations of the energy of the single pion state at a given momentum $\mathbf{p} = \frac{2\pi}{L}\mathbf{n}$ (where $\mathbf{n}$ is an integer triplet) allow for a determination of ξ, and hence establish the single-particle energy-momentum relation that is crucial for determining the scattering amplitude from the location of two-particle energy eigenvalues. We obtain $\xi = 3.469(11)$ where the statistical and systematic uncertainties have been combined in quadrature. This is consistent with the value determined by Dudek *et al.* of $\xi = 3.459(4)$ [18]. A fit to a higher order polynomial provides a result that is consistent with this value but with larger uncertainties in the contributing terms. It is important to use the lattice determined value of ξ, and to propagate its associated uncertainty, as small variations in this parameter are amplified in the determination of the scattering amplitude from two-particle energy eigenvalues when the interaction is weak (and the energy of the two-particle state is consequently near that of the noninteracting system).

III. THE FINITE VOLUME METHODOLOGY

The formalism that was put in place by Lüscher to extract two-particle scattering amplitudes below the inelastic threshold from the energy eigenvalues of two-particle systems at rest in a finite cubic volume [27,28] was extended to systems with nonzero total momentum by Rummukainen and Gottlieb [30]. Subsequent derivations have verified and extended [15,31–34] the work in that paper. The use of boosted systems allows for the amplitude to be determined at more values of momentum (in the CoM), between those defined by $\frac{2\pi}{L}\mathbf{n}$. Here the results that are relevant to the present analysis of the boosted $\pi^+\pi^+$ systems, and to systems at rest, are restated.

Using the notation of Ref. [31], the energy in the CoM frame is denoted by E^*, which is related to the energy E and momentum $\mathbf{P}_{\rm cm}$ in the "laboratory system" (the total lattice momentum) by $E^{*2} = E^2 - |\mathbf{P}_{\rm cm}|^2$. In what follows, it is useful to define $P_{\rm cm} = |\mathbf{P}_{\rm cm}|$. The γ-factor is straightforwardly defined by $\gamma = E/E^*$, and E^* is also related to the magnitude of the momentum of each π^+ in

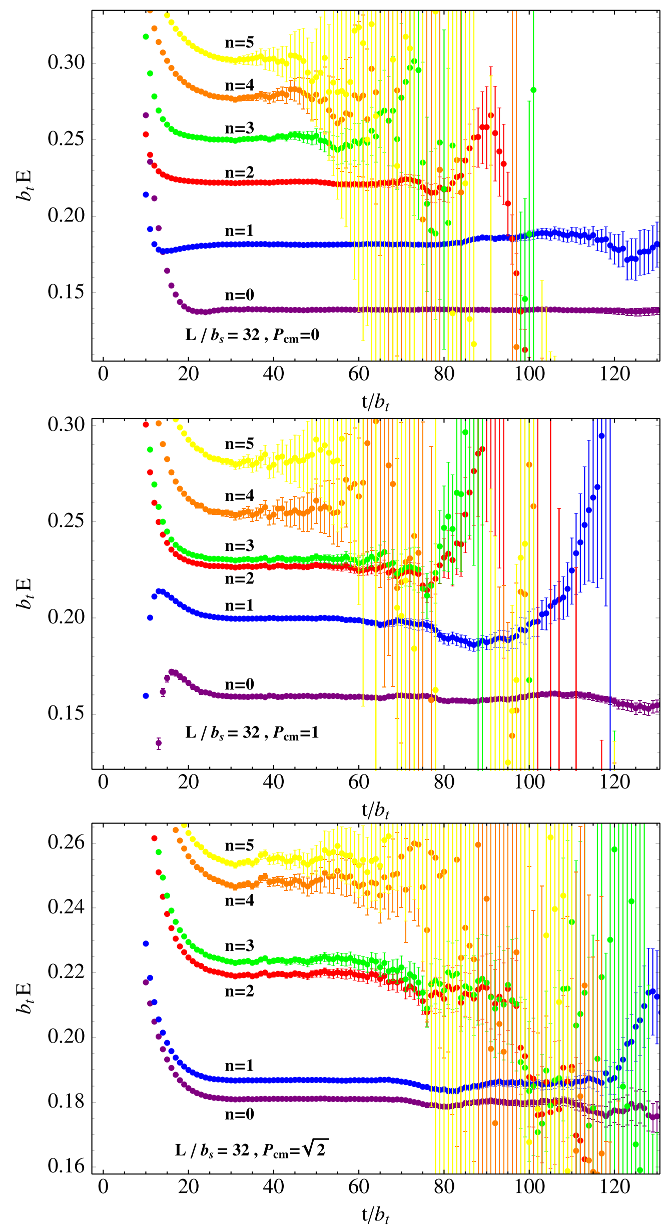

FIG. 1 (color online). The two-pion EMP's for the first six levels (here n indicates the level) with $P_{\rm cm} = 0$ (top), 1 (middle) and $\sqrt{2}$ (bottom) in units of the temporal lattice spacing on the $32^3 \times 256$ ensemble. Only one half of the temporal lattice points are shown.

the CoM frame q^* by $E^{*2} = 4[q^{*2} + m_\pi^2]$. The real part of the inverse of the s-wave scattering amplitude below inelastic threshold, and hence the scattering phase shift, can be extracted from the total energy of the two-particle system with total momentum $\mathbf{P}_{\rm cm} = \frac{2\pi}{L}\mathbf{d}$ in the finite volume via the generalized Lüscher eigenvalue relation

$$q^* \cot\delta(q^*) = \frac{2}{\gamma L\sqrt{\pi}} Z_{00}^{\mathbf{d}}(1;\tilde{q}^{*2}), \tag{2}$$

where the dimensionless quantity $\tilde{q}^*$ is defined by $\tilde{q}^* = \frac{L}{2\pi}q^*$. The function $Z_{00}^{\mathbf{d}}(1;\tilde{q}^{*2})$ is a generalization of the functions defined by Lüscher [27,28],

$$Z_{\rm LM}^{\mathbf{d}}(1;\tilde{q}^{*2}) = \sum_{\mathbf{r}} \frac{|\mathbf{r}|^L Y_{\rm LM}(\Omega_{\mathbf{r}})}{|\mathbf{r}|^2 - \tilde{q}^{*2}}, \tag{3}$$

where the $Y_{\rm LM}$ are spherical harmonics and the sum is over vectors defined by

$$\mathbf{r} = \frac{1}{\gamma}\left(\mathbf{n}_\parallel - \frac{1}{2}\mathbf{d}\right) + \mathbf{n}_\perp = \hat{\gamma}^{-1}\left(\mathbf{n} - \frac{1}{2}\mathbf{d}\right), \tag{4}$$

which in turn are related to the lattice momentum-vectors by $\mathbf{k} = \frac{2\pi}{L}\mathbf{n} = \frac{2\pi}{L}(\mathbf{n}_\parallel + \mathbf{n}_\perp)$. The $\mathbf{n}$ are triplets of integers and the decomposition of $\mathbf{n}$ is along the direction defined by the boost-vector $\mathbf{d}$. Lüscher presented a method [27,28] which can be used [30] to accelerate the numerical evaluation of the sum in Eq. (3), and a generalization of that method leads to

$$\begin{aligned} Z_{\rm LM}^{\mathbf{d}}(1;\tilde{q}^{*2}) = {}& \sum_{\mathbf{r}} \frac{e^{-\Lambda(|\mathbf{r}|^2-\tilde{q}^{*2})}}{|\mathbf{r}|^2 - \tilde{q}^{*2}} |\mathbf{r}|^L Y_{\rm LM}(\Omega_{\mathbf{r}}) \\ & + \delta_{L,0} Y_{00}\gamma\pi^{3/2}\left[2\tilde{q}^{*2}\int_0^\Lambda dt \frac{e^{t\tilde{q}^{*2}}}{\sqrt{t}} \right. \\ & \left. - \frac{2}{\sqrt{\Lambda}} e^{\Lambda\tilde{q}^{*2}}\right] + \gamma \sum_{\mathbf{w}\neq\mathbf{0}} e^{-i\pi\mathbf{w}\cdot\mathbf{d}} |\hat{\gamma}\mathbf{w}|^L Y_{\rm LM}(\Omega_{\hat{\gamma}\mathbf{w}}) \\ & \times \int_0^\Lambda dt \left(\frac{\pi}{t}\right)^{3/2+L} e^{t\tilde{q}^{*2}} e^{-(\pi^2|\hat{\gamma}\mathbf{w}|^2/t)}, \end{aligned} \tag{5}$$

where

$$\hat{\gamma}\mathbf{w} = \gamma\mathbf{w}_\parallel + \mathbf{w}_\perp. \tag{6}$$

The value of the sum is independent of the choice of Λ, and $\Lambda = 1$ has been used in previous works [15].

The energy-level structure resulting from $Z_{00}^{\mathbf{d}}(1;\tilde{q}^{*2})$ has been discussed previously, e.g. Ref. [30]. For the present calculations of boosted systems it is important to identify the closely spaced energy levels. This is because the amplitudes extracted from such levels are subject to large systematic and statistical uncertainties due to the rapid variation of $Z_{00}^{\mathbf{d}}(1;\tilde{q}^{*2})$ in their vicinity, and also due to the difficulty in separating the states contributing to the correlation functions. The energy levels associated with two noninteracting particles are located at the poles of $Z_{00}^{\mathbf{d}}(1;\tilde{q}^{*2})$, and Eq. (4) gives

$$\begin{aligned} &\mathbf{d} = (0,0,0){:}\ \tilde{q}^{*2} = 0, 1, 2, 3, 4, 5, \ldots \\ &\mathbf{d} = (0,0,1){:}\ \tilde{q}^{*2} \\ &\quad = \frac{1}{4\gamma^2}, \frac{4\gamma^2+1}{4\gamma^2}, \underbrace{\frac{9}{4\gamma^2}, \frac{8\gamma^2+1}{4\gamma^2}}, \frac{4\gamma^2+9}{4\gamma^2}, \\ &\quad \frac{16\gamma^2+1}{4\gamma^2}, \ldots \\ &\mathbf{d} = (0,1,1){:}\ \tilde{q}^{*2} = \underbrace{\frac{1}{2\gamma^2}, \frac{1}{2}}, \underbrace{\frac{2\gamma^2+1}{2\gamma^2}, \frac{3}{2}}, \underbrace{\frac{4\gamma^2+1}{2\gamma^2}, \frac{4+\gamma^2}{2\gamma^2}}, \ldots, \end{aligned} \tag{7}$$

and so forth, where the underbraces denote states that become degenerate as $\gamma \to 1$. We stress that the relations summarized in this section are only valid below inelastic threshold.

TABLE II. Results from the lattice QCD calculations of $\pi^+\pi^+$ scattering in the four lattice volumes. $P_{\rm cm}$ denotes the magnitude of the momentum of the center-of-mass in units of $2\pi/L$. In the column denoted by "level", g.s. denotes the ground state, 1st denotes the first excited state and 2nd denotes the second excited state.

k^2/m_π^2	$L^3 \times T$	$P_{\rm cm}$	level	$k\cot\delta/m_\pi$	δ
0.006 78(54)(81)	$32^3 \times 256$	0	$n=0$	−4.49(35)(52)	−1.06(12)(18)
0.017 72(14)(23)	$24^3 \times 128$	0	$n=0$	−4.24(32)(49)	−1.82(19)(30)
0.0309(17)(27)	$20^3 \times 128$	0	$n=0$	−4.25(21)(34)	−2.37(18)(29)
0.0715(32)(48)	$16^3 \times 128$	0	$n=0$	−3.80(15)(22)	−4.03(25)(35)
0.1641(20)(23)	$32^3 \times 256$	1	$n=0$	−3.33(38)(48)	−7.1(0.8)(1.0)
0.378(5)(11)	$20^3 \times 128$	1	$n=0$	−4.1(0.4)(1.0)	−8.6(0.8)(3.6)
0.3838(42)(85)	$32^3 \times 256$	$\sqrt{2}$	$n=0$	−1.65(12)(28)	−20.6(1.5)(3.1)
0.7323(53)(88)	$32^3 \times 256$	0	$n=1$	−2.78(29)(57)	−17.2(1.7)(2.9)
0.9233(51)(73)	$32^3 \times 256$	1	$n=1$	−2.14(16)(26)	−24.1(1.6)(2.6)
1.373(13)(22)	$24^3 \times 128$	0	$n=1$	−2.10(19)(36)	−29.2(2.3)(4.3)
1.582(9)(16)	$32^3 \times 256$	0	$n=2$	−1.19(09)(14)	−46.5(2.3)(3.5)
1.969(02)(04)	$20^3 \times 128$	0	$n=1$	−2.33(32)(56)	−31.6(3.5)(5.6)

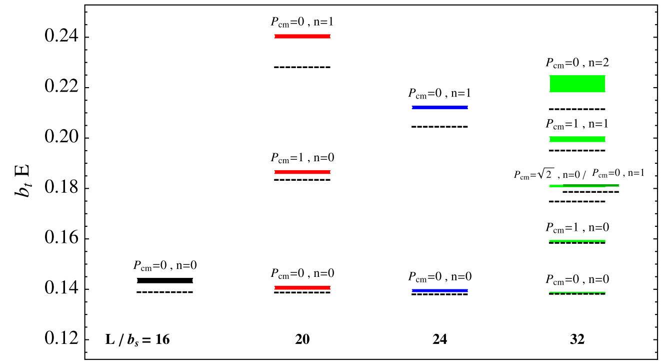

FIG. 2 (color online). The two-pion energies in units of the temporal lattice spacing for the lattice ensembles considered in this work. The (vertical) thickness of each level indicates the uncertainty of the energy determination. Each state is labeled according to its center-of-mass momentum $P_{\rm cm}$, and its excitation level n. The noninteracting levels are denoted by dashed (black) lines. Notice that the $32^3 \times 256$ $P_{\rm cm} = \sqrt{2}$, $n = 0$ and $P_{\rm cm} = 0$, $n = 1$ levels are nearly degenerate.

IV. $\pi^+\pi^+$ SCATTERING ON THE LATTICE

A. Lattice phase shift

The scattering of pions in the $I = 2$ channel is perturbative at low momentum and at small light-quark masses, as guaranteed by χPT. In a finite volume, this translates into two-pion energies that deviate only slightly from the noninteracting energies; i.e., the sum of the pion masses (or boosted pion masses for moving systems). We have analyzed $\pi^+\pi^+$ correlation functions with $P_{\rm cm} = 0, 1, \sqrt{2}$ (in

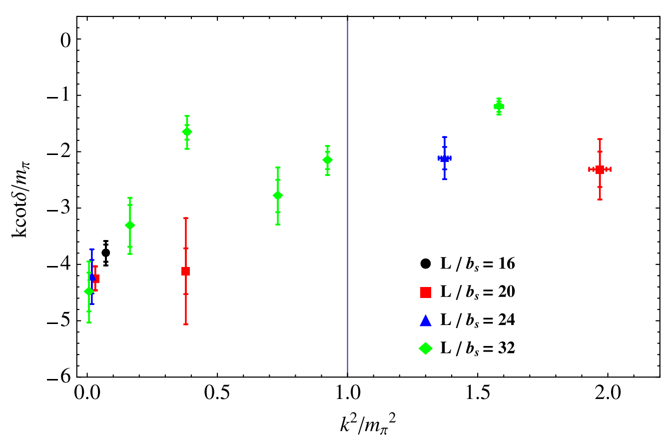

FIG. 3 (color online). Results of the lattice QCD calculations processed through the energy-eigenvalue relation to give values of $k\cot\delta/m_\pi$. The {circles, squares, triangles, diamonds} ({black, red, blue, green}) correspond to the ensembles $\{16^3 \times 128, 20^3 \times 128, 24^3 \times 128, 32^3 \times 256\}$. Statistical and systematic uncertainties are shown as the inner and outer error-bars, respectively. The vertical (blue) line at $k^2 = m_\pi^2$ indicates the limit of the range of validity of the ERE set by the t-channel cut. The inelastic threshold is at $k^2 = 3m_\pi^2$.

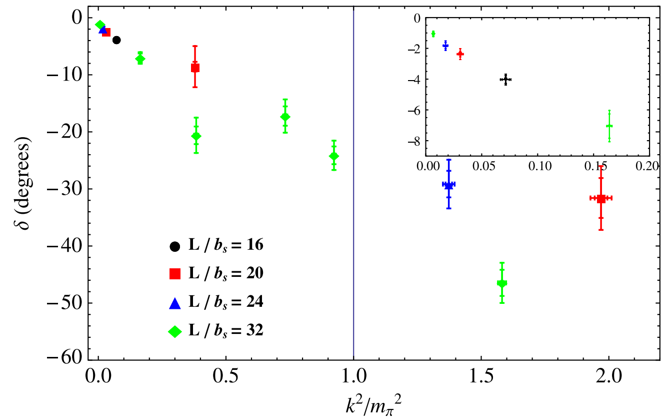

FIG. 4 (color online). Results of the lattice QCD calculations processed through the energy-eigenvalue relation to give values of the phase shift δ. The phase shift at low energies is shown as an inset. The {circles, squares, triangles, diamonds} ({black, red, blue, green}) correspond to the ensembles $\{16^3 \times 128, 20^3 \times 128, 24^3 \times 128, 32^3 \times 256\}$. Statistical and systematic uncertainties are shown as the inner and outer error-bars, respectively. The vertical (blue) line at $k^2 = m_\pi^2$ indicates the limit of the range of validity of the ERE set by the t-channel cut. The inelastic threshold is at $k^2 = 3m_\pi^2$.

units of $\frac{2\pi}{L}$) and with various (noninteracting) momentum projections among the pions. It is straightforward to partially diagonalize this system of correlation functions into the energy eigenstates at intermediate and long times. This is achieved by assuming that the two-pion energy levels are close to their noninteracting values, and then varying the linear combination of correlation functions in order to maximize the plateau region. (Coupled exponential fits to the various correlators with the same $P_{\rm cm}$ lead to consistent determinations). As an example, in Fig. 1 we show the two-pion effective mass plots (EMP's) on the $32^3 \times 256$ ensemble with $P_{\rm cm} = 0, 1, \sqrt{2}$. Six energy levels can be clearly identified in the EMP's in Fig. 1 for each of the values of $P_{\rm cm}$. [Note that these levels clearly show the near degeneracies of the noninteracting system as established in Eq. (7)]. However, only the first few levels, when propagated through the eigenvalue equation, lead to statistically significant values for the phase shift. While the energies of other levels are established, the structure of the eigenvalue

TABLE III. ERE parameters extracted from the lattice QCD calculations of $k\cot\delta/m_\pi$.

Quantity	Fit A: $k^2/m_\pi^2 < 0.5$	Fit B: $k^2/m_\pi^2 < 1$
$m_\pi a$	0.230(10)(16)	0.226(10)(16)
$m_\pi r$	12.9(1.5)(2.9)	18.1(2.4)(4.7)
$m_\pi^2 ar$	2.95(20)(42)	4.06(30)(57)
P	-	−0.001 23(30)(55)
χ^2/dof	0.83	0.79

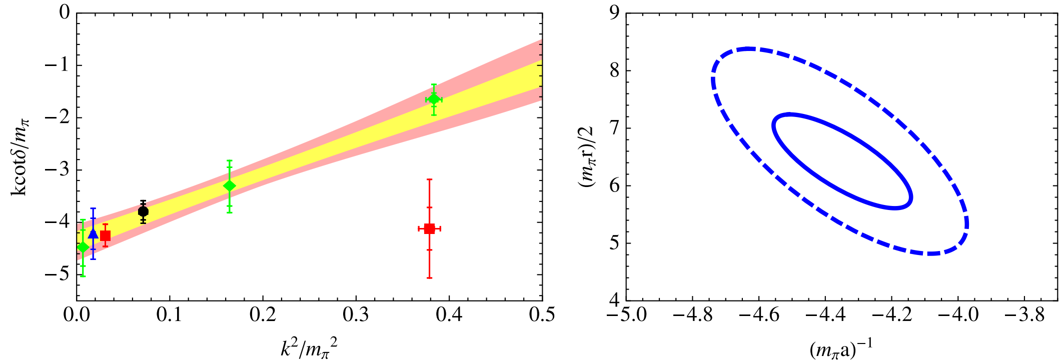

FIG. 5 (color online). Left panel: a two-parameter fit to $k\cot\delta/m_\pi$ over the region $k^2/m_\pi^2 < 0.5$ (fit A). The {circles, squares, triangles, diamonds} ({black, red, blue, green}) correspond to the $\{16^3\times 128,\ 20^3\times 128,\ 24^3\times 128,\ 32^3\times 256\}$ ensembles. The shaded bands correspond to statistical (inner-yellow) and statistical and systematic added in quadrature (outer-pink). Right panel: 68% confidence interval error ellipses in the $(m_\pi a)^{-1}$-$\frac{1}{2}m_\pi r$ space. The inner-solid ellipse and the outer-dashed ellipse correspond to the statistical and to the statistical and systematic uncertainties added in quadrature, respectively.

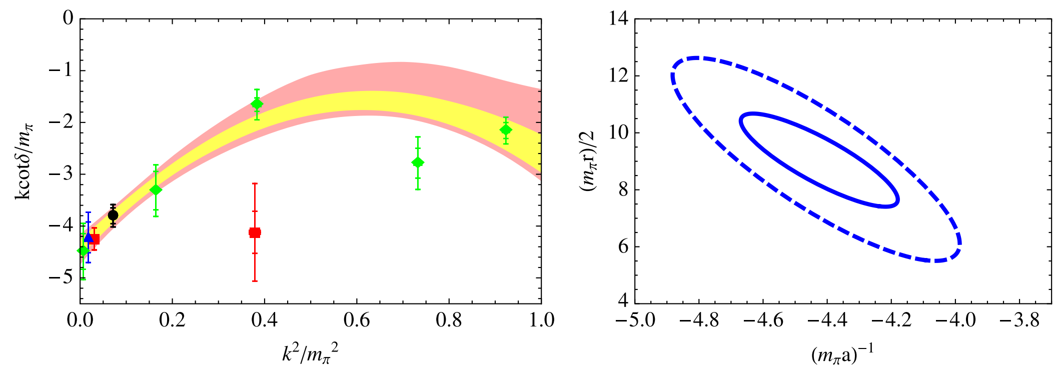

FIG. 6 (color online). Left panel: a three-parameter fit to $k\cot\delta/m_\pi$ over the region $k^2/m_\pi^2 < 1$ (fit B). The {circles, squares, triangles, diamonds} ({black, red, blue, green}) correspond to the $\{16^3\times 128,\ 20^3\times 128,\ 24^3\times 128,\ 32^3\times 256\}$ ensembles. The shaded bands correspond to statistical (inner-yellow) and statistical and systematic added in quadrature (outer-pink). Right panel: 68% confidence interval error ellipses in the $(m_\pi a)^{-1}$-$\frac{1}{2}m_\pi r$ space. The inner-solid ellipse and the outer-dashed ellipse correspond to the statistical and to the statistical and systematic uncertainties added in quadrature, respectively.

equation is such that the uncertainties, as small as they appear, are sufficiently large to produce uncertainties in the amplitude that are too large and preclude statistical significance.[1] The states that have been analyzed to produce amplitudes and phase shifts are given in Table II, and are shown in Fig. 2. Note that momenta are quoted in units of m_π in order to formulate the subsequent analysis in a manner that is independent of the scale setting. The values of $k\cot\delta/m_\pi$ and δ resulting from the energy eigenvalues are shown in Fig. 3 and Fig. 4, respectively.

Note that while the $32^3\times 256$ $P_{\rm cm}=\sqrt{2}$, $n=0$ and $20^3\times 128$ $P_{\rm cm}=0$, $n=1$ levels appear discrepant, we believe this is likely a statistical fluctuation. Also, the phase shift we have extracted from the first excited state in the $24^3\times 128$ ensemble disagrees with the equivalent extraction presented in Ref. [18]. While we find a phase shift of $\delta = -29.2 \pm 2.3 \pm 4.3^o$ at $k^2 \sim 0.21\ \mathrm{GeV}^2$, Ref. [18] finds $\delta \sim -13 \pm 2^o$ at $k^2 \sim 0.2\ \mathrm{GeV}^2$. Our result is consistent with the phase shifts at the nearby momenta calculated on the $32^3\times 256$ ensemble.

B. The effective range expansion parameters

The ERE is an expansion of the real part of the inverse scattering amplitude in powers of the CoM energy,

$$\frac{k\cot\delta}{m_\pi} = -\frac{1}{m_\pi a} + \frac{1}{2}m_\pi r\left(\frac{k^2}{m_\pi^2}\right) + P(m_\pi r)^3\left(\frac{k^2}{m_\pi^2}\right)^2 + \ldots, \qquad (8)$$

[1]The EMPs of Fig. 1 indicate that the signal-to-noise ratio of the two-pion correlation functions decreases with increasing excitation number.

where $m_\pi a$ and $m_\pi r$ are the scattering length and effective range in units of m_π^{-1}, and P is the shape parameter.[2] Here $k = |\mathbf{k}|$ is the magnitude of each pion's momentum in the CoM. Such an expansion is expected to be convergent for energies below the t-channel cut, which is set by $\pi\pi$ exchange in the t channel. The t-channel cut starts at $k^2 = m_\pi^2$, while the inelastic threshold is $k^2 = 3m_\pi^2$.

As the calculations of $k\cot\delta/m_\pi$ are approximately linear in k^2 in the region $k^2/m_\pi^2 < 0.5$, the scattering length and the effective range are fit (fit A) using Eq. (8) with P and the other higher order terms set to zero. The extracted values of $m_\pi a$ and $m_\pi r$ are given in Table III, and the resulting fit is shown in Fig. 5, along with the 68% confidence interval error ellipses for the two-parameters. In the region $k^2/m_\pi^2 < 1$ the lattice QCD calculations exhibit curvature consistent with quadratic (and higher) dependence on k^2. In fit B the three leading ERE parameters are fit to the results of the lattice QCD calculations. The fits are compared to the lattice QCD calculations in Fig. 6, which also shows the 68% confidence interval error ellipse for the two-parameter subspace of the three-parameter fit. It is clear from Table III that the fit parameters are consistent within the combined statistical and systematic uncertainties. In what follows, where we use χPT to predict the parameters at the physical point, the spread in value of the ERE parameters will serve as a useful gauge of the systematic uncertainty introduced in the fitting of the scattering amplitude. It is noteworthy that the data allows a significant determination of the shape parameter, P.

V. CHIRAL INTERPOLATIONS

A. Motivation

Although these lattice QCD calculations have been performed only at one value of the pion mass, as we will see, the effective range and threshold scattering parameters satisfy low-energy theorems mandated by chiral symmetry, and therefore each scattering parameter can be used to fix the corresponding LEC that appears at NLO in χPT. Thus the scattering parameters at the physical point can be predicted at NLO in χPT. This is, in a sense, a chiral interpolation rather than an extrapolation since one is interpolating between the pion mass of the lattice QCD calculation and the chiral limit. Unfortunately, the pion decay constant, f_π, has not yet been accurately computed on the anisotropic lattice ensembles that have been used in this work. However, χPT and the results of mixed-action lattice QCD calculations [43] can be used to determine f_π (and its uncertainty) evaluated at the pion mass of the present lattice QCD calculations up to lattice spacing artifacts. Specifically, in what follows we use $\sqrt{z^{\rm latt}} \equiv m_\pi^{\rm latt}/f_\pi^{\rm latt} = 2.59(13)$ at $m_\pi \sim 390$ MeV.

B. Threshold parameters in χPT

The relation between the $\pi^+\pi^+$ s-wave scattering amplitude $t(s)(= t_{L=0}^{I=2}(s))$ and the phase shift δ is given by [4]

$$t(s) = \left(\frac{s}{s-4}\right)^{1/2}\frac{1}{2i}\{e^{2i\delta(s)} - 1\}, \tag{9}$$

where $s = 4(1 + k^2/m_\pi^2)$ and $k = |\mathbf{k}|$ is the magnitude of the three-momentum of each π^+ in the CoM frame. The NLO scattering amplitude can be expressed in terms of three LEC's, C_1, C_2, and C_4 [2,3]:

$$\begin{aligned} t(k) = &-\frac{m_\pi^2}{8\pi f_\pi^2} - \frac{m_\pi^4}{f_\pi^4}\left(C_1 - \frac{31}{384\pi^3}\right) + \frac{k^2}{f_\pi^2}\left[-\frac{1}{4\pi} + \frac{m_\pi^2}{f_\pi^2}\left(\frac{301}{1152\pi^3} - \frac{1}{128\pi^2}C_2 - \frac{7}{2}C_1\right)\right] \\ &+ \frac{k^4}{f_\pi^4}\left[\frac{14}{45\pi^3} - \left(\frac{19}{8}C_1 - \frac{9}{512\pi^2}C_2 + 216\pi C_4\right)\right] - \frac{1}{4\pi^3 f_\pi^4}\left(\frac{3}{32}m_\pi^4 + \frac{5}{12}m_\pi^2k^2 + \frac{5}{9}k^4\right)\log\left(\frac{m_\pi^2}{f_\pi^2}\right) \\ &+ \frac{1}{16\pi^3 f_\pi^4}\left(\frac{1}{4}m_\pi^4 + m_\pi^2k^2 + k^4\right)\sqrt{\frac{k^2}{k^2+m_\pi^2}}\log\left(\frac{\sqrt{\frac{k^2}{k^2+m_\pi^2}} - 1}{\sqrt{\frac{k^2}{k^2+m_\pi^2}} + 1}\right) + \frac{1}{8\pi^3 f_\pi^4}\left(\frac{3}{16}m_\pi^4 + \frac{7}{9}m_\pi^2k^2 + \frac{11}{18}k^4\right) \\ &\times\sqrt{\frac{k^2+m_\pi^2}{k^2}}\log\left(\frac{\sqrt{\frac{k^2+m_\pi^2}{k^2}} - 1}{\sqrt{\frac{k^2+m_\pi^2}{k^2}} + 1}\right) - \frac{m_\pi^4}{128\pi^3 f_\pi^4}\left(1 + \frac{13}{12}\frac{m_\pi^2}{k^2}\right)\log^2\left(\frac{\sqrt{\frac{k^2+m_\pi^2}{k^2}} - 1}{\sqrt{\frac{k^2+m_\pi^2}{k^2}} + 1}\right). \end{aligned} \tag{10}$$

The C_i can be expressed in terms of the $l_i \equiv l_i^r(\mu = f_\pi)$, the familiar low-energy constants of two-flavor χPT [2],

$$\begin{aligned} &C_1 \equiv -\frac{1}{2\pi}(4l_1 + 4l_2 + l_3 - l_4) - \frac{1}{128\pi^3}; \qquad C_2 \equiv 32\pi(12l_1 + 4l_2 + 7l_3 - 3l_4) + \frac{31}{6\pi}; \\ &C_4 \equiv \frac{1}{5184\pi^2}(212l_1 + 40l_2 + 123l_3 - 69l_4) + \frac{701}{622\,080\pi^4}. \end{aligned} \tag{11}$$

The behavior of the amplitude near threshold ($k^2 \to 0$) can be written as a power-series expansion in the CoM energy

[2] For a modern discussion of the effective range expansion and its regime of validity, see Ref. [29].

$$\mathrm{Re}\, t(k) = -m_\pi a + k^2 b + k^4 c + O(k^6), \tag{12}$$

where the threshold parameters b and c are referred to as slope parameters. Matching the threshold expansion in Eq. (12) to the ERE in Eq. (8) gives [4]:

$$m_\pi r = -\frac{1}{m_\pi a} - \frac{2m_\pi^2 b}{(m_\pi a)^2} + 2m_\pi a; \tag{13}$$

$$P = -\frac{(m_\pi a)^3[(m_\pi a)^2 - 4(m_\pi a)^4 + 8(m_\pi a)^6 - 4(m_\pi a + 2(m_\pi a)^3)bm_\pi^2 - 8(b^2 + m_\pi ac)m_\pi^4]}{8(m_\pi a - 2(m_\pi a)^3 + 2bm_\pi^2)^3}. \tag{14}$$

These equations can be inverted to obtain b and c from the lattice-determined ERE parameters. Expanding the NLO amplitude in Eq. (10) in powers of k, one finds NLO χPT expressions for the ERE and threshold parameters:

$$\begin{aligned} &m_\pi a = \frac{z}{8\pi} + z^2 C_1 + \frac{3z^2}{128\pi^3}\log z, \qquad m_\pi r = \frac{24\pi}{z} + C_2 + \frac{17}{6\pi}\log z, \qquad m_\pi^2 a r = 3 + zC_3 + \frac{11z}{12\pi^2}\log z,\\ &P = -\frac{23z^2}{13\,824\pi^2} + z^3 C_4 + \frac{613z^3}{995\,328\pi^4}\log z, \qquad m_\pi^2 b = -\frac{z}{4\pi} - z^2\left(\frac{7}{2}C_1 + \frac{1}{128\pi^2}C_2 + \frac{5}{48\pi^3}\log z\right),\\ &m_\pi^4 c = -z^2\left(\frac{19}{8}C_1 - \frac{9}{512\pi^2}C_2 + 216\pi C_4 + \frac{5}{36\pi^3}\log z\right), \end{aligned} \tag{15}$$

where $z \equiv m_\pi^2/f_\pi^2$ and $C_3 = 24\pi C_1 + \frac{1}{8\pi}C_2$. It is important to note that the shape parameter P and the threshold parameter c do not receive contributions from LO χPT; i.e., they vanish in current algebra.

C. Chiral interpolation of threshold parameters

Using the ERE parameter set from fit B given in Table III, with statistical and systematic uncertainties combined in quadrature, the four functions $C_1((m_\pi a)^{\mathrm{latt}}, z^{\mathrm{latt}})$, $C_2((m_\pi r)^{\mathrm{latt}}, z^{\mathrm{latt}})$, $C_3((m_\pi^2 ar)^{\mathrm{latt}}, z^{\mathrm{latt}})$, $C_4(P^{\mathrm{latt}}, z^{\mathrm{latt}})$ can be determined. The ERE parameters in Table III give

$$C_1^{\mathrm{NLO}} = -0.002\,37(52), \qquad C_2^{\mathrm{NLO}} = 5.2(5.2); \\ C_3^{\mathrm{NLO}} = -0.02(0.10), \qquad C_4^{\mathrm{NLO}} = 9.0(4.0)\times 10^{-6}, \tag{16}$$

where the superscripts denote that these constants are evaluated at NLO in χPT, and from which follow, using Eq. (15), the predictions at the physical point[3] of

$$\begin{aligned} m_\pi a &= 0.0417(07)(02)(16),\\ m_\pi r &= 72.0(5.3)(5.3)(2.7),\\ m_\pi^2 ar &= 2.96(11)(17)(11),\\ P &= -2.022(58)(12)(76)\times 10^{-4},\\ b &= -0.832(50)(0)(31)\times 10^{-1} m_\pi^{-2},\\ c &= 0.013(33)(01)(0) m_\pi^{-4}, \end{aligned} \tag{17}$$

where the first systematic uncertainty has been estimated by comparing the interpolated results of Fits A and B, and by "pruning" the highest energy datum from the lattice QCD results and refitting. The second systematic uncertainty contains estimates, using naive dimensional analysis, of the effects from higher orders in the chiral expansion, next-to-next-to-leading order (NNLO) and higher, as well as the contributions from lattice spacing artifacts that are expected to contribute at $\mathcal{O}(b_s^2)$ [44]. The chiral interpolation of $m_\pi^2 ar$ is shown in Fig. 7. (Note that the band in Fig. 7 represents fit B, and the outer uncertainty on the interpolated result represents the effect of the two

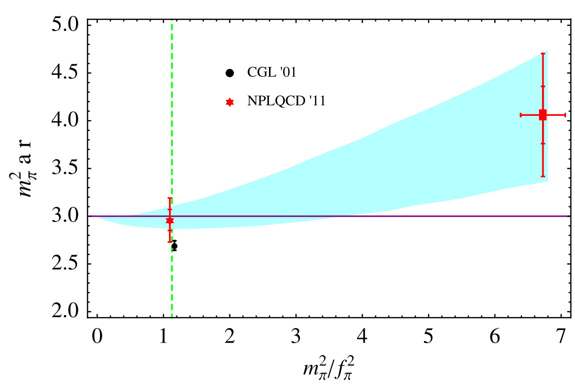

FIG. 7 (color online). The dashed (green) line denotes the physical line, and the horizontal solid (purple) line denotes the LO χPT prediction, which is $m_\pi^2 ar = 3$ in the chiral limit. The band denotes the 68% confidence interval interpolation of the results of the lattice calculation (the (red) rectangle) from fit B. The lattice QCD + χPT prediction at the physical point is the (red) star on the physical line, and the Roy equation prediction [8] is the (black) circle on the physical line.

[3]Note that the precise NPLQCD result for the scattering length, $m_\pi a = -0.043\,30(42)$, computed in Ref. [12] with domain-wall valence quarks on staggered sea quarks, is more precise than the result of Eq. (17).

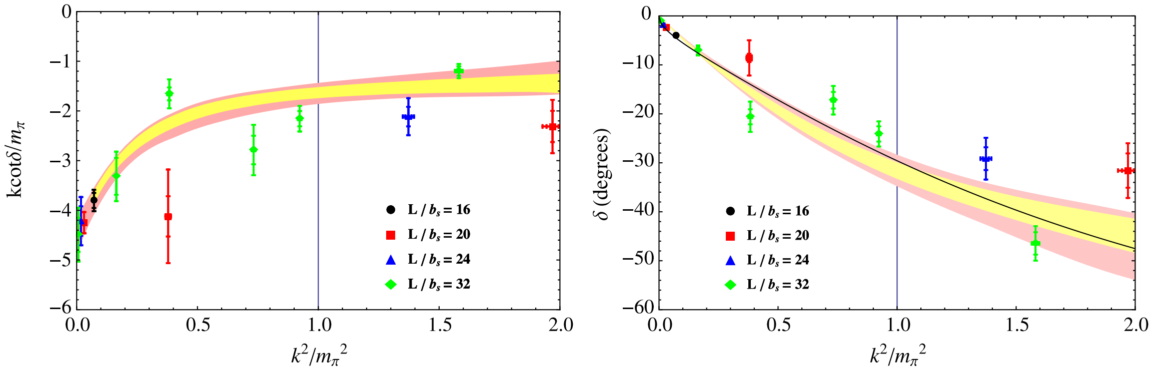

FIG. 8 (color online). Three parameter fit (C_1, C_2, and C_4) of the NLO χPT expression for $k\cot\delta/m_\pi$ to the results of the lattice QCD calculations. The shaded bands correspond to statistical (inner-yellow) uncertainties and statistical and systematic uncertainties added in quadrature (outer-pink). The solid (black) curve in the right panel is the LO χPT prediction (current algebra) at the pion mass used in the lattice QCD calculations, $m_\pi \sim 390$ MeV.

systematic uncertainties and the statistical uncertainty added in quadrature, as described above).

With Eq. (11), the fit values of the C_i in Eq. (16) can be used to constrain various combinations of the l_i, and the renormalization group can be used to express these constraints in terms of the scale-independent dimensionless barred quantities, the $\bar{l}_i$ [2].[4] We find that

$$\bar{l}_3 - 4\bar{l}_4 = -29(27), \qquad \bar{l}_1 - 6\bar{l}_4 = -32(25)$$
$$2\bar{l}_1 - 3\bar{l}_3 = 28(29), \qquad \bar{l}_1 + 4\bar{l}_2 = 15.8(6.7), \tag{18}$$

where statistical and systematic uncertainties have been combined in quadrature. With increased precision in the determination of the ERE parameters, such determinations of the LECs could become competitive with other methods.

These results may seem surprisingly accurate for a lattice QCD calculation performed at a single pion mass. As mentioned previously, it is the chiral symmetry constraints on the scattering parameters in the approach to the chiral limit that is responsible for the precision. The scattering length obtained here is consistent within uncertainties with the previous lattice QCD determinations [11–13]. Further, the scattering length and threshold parameters are found to agree with determinations from the Roy equation (with chiral symmetry input) [8],

$$m_\pi a = 0.0444(10), \qquad b = -0.803(12) \times 10^{-1} m_\pi^{-2};$$
$$m_\pi^2 a r = 2.666(0.083), \tag{19}$$

at the 1σ-level. Figure 7 provides a comparison of the lattice calculation (and interpolation) and the Roy equation value of $m_\pi^2 a r$.

[4]The l_i are related to the $\bar{l}_i$ via

$$l_i = \frac{\gamma_i}{32\pi^2}\left(\bar{l}_i + \log\left(\frac{m_\pi^2}{\mu^2}\right)\right),$$

where $\gamma_1 = \frac{1}{3}$, $\gamma_2 = \frac{2}{3}$, $\gamma_3 = -\frac{1}{2}$ and $\gamma_4 = 2$.

D. Chiral interpolation of the phase shift

The $\pi^+\pi^+$ scattering phase shifts calculated with lattice QCD, which extend above the range of validity of the ERE but remain below the inelastic threshold, can be used to predict the phase shift at the physical value of the pion mass. While the chiral expansion may break down for scattering at sufficiently high energies, we ignore this issue and fit the NLO χPT amplitude (one-loop level) to the results of the lattice QCD calculations at all of the calculated energies, the maximum invariant mass being $\sqrt{s} \sim 1340$ MeV.

The results of the lattice QCD calculations given in Table II are fit to the formula

$$\frac{k\cot\delta}{m_\pi} = \sqrt{1 + \frac{k^2}{m_\pi^2}}\left(\frac{1}{t_{\rm LO}(k)} - \frac{t_{\rm NLO}(k)}{(t_{\rm LO}(k))^2}\right) + i\frac{k}{m_\pi}, \tag{20}$$

where $t_{\rm LO}$ and $t_{\rm NLO}$ are the LO and NLO contributions to $t(k)$ in the chiral expansion, given in Eq. (10). The result of the fit is shown in Fig. 8; in the left panel the fit (of C_1, C_2, and C_4) to $k\cot\delta/m_\pi$ is shown, and in the right panel, the fit values of C_1, C_2, and C_4 (fully correlated) are used to predict the phase shift at the pion mass of the lattice QCD calculations, $m_\pi \sim 390$ MeV. The 68% confidence intervals for C_1, C_2, and C_4 from this fit are

$$C_1^{\rm NLO} = (-0.0040, -0.0013), \qquad C_2^{\rm NLO} = (2.67, 24.1),$$
$$C_4^{\rm NLO} = (-1.7, +3.6) \times 10^{-5}, \tag{21}$$

with a $\chi^2/\text{dof} = 2.1$ (for the fit with the statistical and systematic uncertainties combined in quadrature). The interpolated ERE parameters are

$$m_\pi a = 0.0412(08)(16), \qquad m_\pi r = 80.0(9.58)(3.0),$$
$$P = -1.85(31)(07) \times 10^{-4}, \tag{22}$$

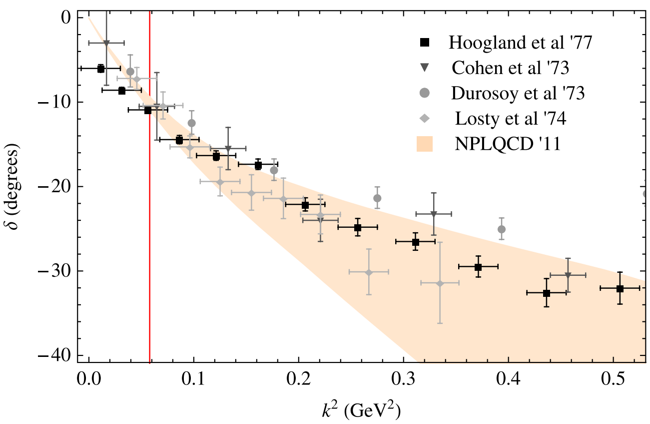

FIG. 9 (color online). The shaded band is the lattice QCD prediction of the phase shift at the physical value of the pion mass, $m_\pi \sim 140$ MeV using NLO χPT with the statistical and systematic uncertainties combined in quadrature. The data is experimental (black and grey) taken from Refs. [45–48]. The red vertical line denotes the inelastic (4π) threshold.

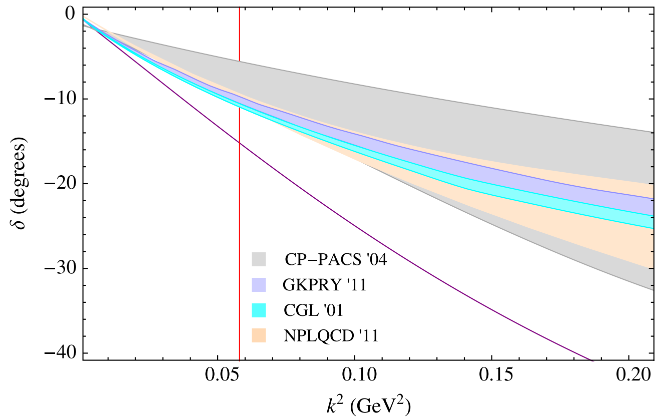

FIG. 10 (color online). The shaded band is the lattice QCD prediction of the phase shift at the physical value of the pion mass, $m_\pi \sim 140$ MeV using NLO χPT with the statistical and systematic uncertainties combined in quadrature. The outer (magenta) band is the CP-PACS physical prediction [15], and the two inner (blue and purple) bands are the Roy equation predictions [8,9]. (Note that the band from Ref. [8] lies above the band from Ref. [9]). The solid (purple) curve is the LO χPT prediction (current algebra) at the physical pion mass. The red vertical line denotes the inelastic (4π) threshold.

which are consistent within uncertainties, but less precise, than the threshold determinations of Eq. (17). Here the second uncertainty is a naive dimensional analysis estimate of the effects of higher orders in the chiral expansion and lattice spacing artifacts. For a better determination of the threshold parameters from the global fit, one requires more accurate lattice QCD calculations and the $\pi^+\pi^+$ amplitude beyond NLO in the chiral expansion. In Fig. 9 the fit values of C_1, C_2, and C_4 are used to predict the phase shift at the physical value of the pion mass, $m_\pi \sim 140$ MeV, which is compared to the experimental data of Refs. [45–48]. Figure 10 compares the phase shift prediction to the lattice QCD phase-shift determination by CP-PACS [15], and the Roy equation determinations of the phase shift from Refs. [8,9]. One should keep in mind that the interpolated phase shift is valid above the inelastic threshold, as the 4π intermediate state appears beyond NLO in the χPT calculation (at two-loop level). The combined lattice QCD and χPT prediction of the $\pi^+\pi^+$ phase shift at the physical pion mass is found to be in good agreement with the experimentally-determined phase shift. While for $|\mathbf{k}| \geq 400$ MeV the uncertainty in the prediction exceeds the uncertainties in the experimental data, below this momentum the lattice QCD + χPT prediction is more precise.

It is interesting to observe that while the LO phase shift well reproduces the results of the lattice QCD calculations at $m_\pi \sim 390$ MeV, as shown in Fig. 8, the NLO contributions are important at the physical pion mass, as seen in Fig. 10. This is to be contrasted with the chiral behavior of the scattering length which is dominated by the LO amplitude, with NLO making a small but noticeable contribution. In an attempt to isolate the origin of this apparent difference, it is useful to consider scattering at NLO in the chiral limit where

$$\cot\delta \rightarrow -\frac{4\pi f_\pi^2}{k^2} + \frac{40}{9\pi}\log\left(\frac{2k}{f_\pi}\right) + 38\pi^2 C_1 - \frac{9}{32}C_2 + 3456\pi^3 C_4 - \frac{224}{45\pi}. \tag{23}$$

The phase shift can be defined this way even in the chiral limit because at LO and NLO the only intermediate states contributing to the scattering amplitude involve two pions. Inelastic channels, such as four-pion intermediate states which would invalidate the relation in Eq. (9), first contribute to the scattering amplitude at NNLO. This is what allows for the phase shift to be predicted above the inelastic threshold, and to remain perturbatively close to the actual value for momenta below the chiral symmetry breaking scale. At LO in the expansion, the phase shift reaches $\delta = \pi/4$ when $k^2 = 4\pi f_\pi^2 \sim 0.22$ GeV^2 (using $f_\pi = 132$ MeV), consistent with the phase shift shown in Fig. 10. Clearly, it is reasonable to take the limit $m_\pi \ll k$ for this value of $k (k \sim 470$ MeV). Further, at this value of k, the NLO terms are approximately equal to the LO terms, providing an estimate of the convergence region of the chiral expansion for the scattering process.

It is also worth noting that while it is formally invalid to use the Lüscher relation in Eq. (2) for the scattering of pions above inelastic threshold, χPT indicates that the error introduced into phase-shift determinations is small, occurring at NNLO in the chiral expansion. This is not expected to be true for other scattering processes (those not involving the pseudo-Goldstone bosons). Therefore, while strictly speaking the results presented in Ref. [18] above inelastic threshold arise from an invalid application of Eq. (2), the expected deviation from the true result is expected to be small (at momenta for which the chiral expansion is converging), suppressed by two orders in the chiral expansion. Clearly, precision calculations of the phase shift above the inelastic threshold cannot rely upon a methodology that does not include the effects of inelastic processes. As all of the calculations in our work are below the inelastic threshold, the present analyses and predictions do not suffer from this inconsistency.

VI. SUMMARY AND CONCLUSION

The increases in high-performance computing capabilities and the advent of powerful new algorithms have thrust lattice QCD into a new era where the interactions among hadrons can be computed with controlled systematic uncertainties. While calculation of the basic properties of nuclei and hypernuclei is now a goal within reach, it is important to consider the simplest hadronic scattering processes as a basic test of the lattice methodology for extracting scattering information (including bound states) from the eigenstates of the QCD Hamiltonian in a finite volume. In this work, we have calculated the $\pi^+\pi^+$ scattering amplitude using lattice QCD over a range of momenta below the inelastic threshold. Our predictions for the threshold scattering parameters, and hence the leading three terms in the ERE expansion, are consistent with determinations using the Roy equations [8,9] and the predictions of χPT. In particular, our determination of $m_\pi^2 ar = 2.96(11)(17)(11)$ from an interpolation of a fit to the low momentum values of $k\cot\delta/m_\pi$ is consistent with the LO prediction of χPT of $m_\pi^2 ar = 3(1 + \mathcal{O}(m_\pi^2/\Lambda_\chi^2))$. Further, the resulting predictions for the phase shift at the physical pion mass—using NLO χPT—are in agreement with experimental data, and are even more precise in the low-momentum region.

The lattice QCD calculations presented here were performed at one lattice spacing simply due to the lack of computational resources, therefore, an extrapolation of the ERE parameters to the continuum limit (as was performed in the work of CP-PACS [15]) could not be performed. The discretization of the quark fields that has been employed gives rise to lattice spacing artifacts at $\mathcal{O}(b_s^2)$, and we expect such contributions to be small for these calculations.

ACKNOWLEDGMENTS

We thank G. Colangelo, H. Leutwyler, J. Nebreda and J. Pelaez for valuable conversations and communications, K. Roche for computing resources at ORNL NCCS and R. Edwards and B. Joo for developing QDP + +, Chroma [49] and production. We acknowledge computational support from the USQCD SciDAC project, NERSC (Office of Science of the DOE, Grant No. DE-AC02-05CH11231), the UW HYAK facility, Centro Nacional de Supercomputación (Barcelona, Spain), LLNL, the Argonne Leadership Computing Facility at Argonne National Laboratory (Office of Science of the DOE, under Contract No. DE-AC02-06CH11357), and the NSF through Teragrid resources provided by TACC and NICS under Grant No. TG-MCA06N025. S. R. B. was supported in part by the NSF under CAREER Grant No. PHY-0645570. The Albert Einstein Center for Fundamental Physics is supported by the Innovations-und Kooperationsprojekt C-13 of the Schweizerische Universitätskonferenz SUK/CRUS. The work of E. C. and A. P. is supported under Contract No. FIS2008-01661 from MEC (Spain) and FEDER. A. P. acknowledges support from the RTN Flavianet under Contract No. MRTN-CT-2006-035482 (EU). H-W. L. and M. J. S. were supported in part by the DOE under Grant No. DE-FG03-97ER4014. W. D. and K. O. were supported in part by the DOE under Grants No. DE-AC05-06OR23177 (J. S. A.) and No. DE-FG02-04ER41302. W. D. was also supported by the DOE OJI under Grant No. DE-SC0001784 and Jeffress Memorial Trust under Grant No. J-968. K. O. was also supported in part by the NSF under Grant No. CCF-0728915 and the DOE OJI under Grant No. DE-FG02-07ER41527. A. T. was supported by the NSF under Grant No. PHY-0555234 and the DOE under Grant No. DE-FC02-06ER41443. The work of T. L. was performed under the auspices of the U.S. Department of Energy by LLNL under Contract No. DE-AC52-07NA27344 and the UNEDF SciDAC under Grant No. DE-FC02-07ER41457. The work of A. W. L. was supported in part by the Director, Office of Energy Research, Office of High Energy and Nuclear Physics, Divisions of Nuclear Physics, of the U.S. DOE under Contract No. DE-AC02-05CH11231.

[1] S. Weinberg, Phys. Rev. Lett. **17**, 616 (1966).
[2] J. Gasser and H. Leutwyler, Ann. Phys. (N.Y.) **158**, 142 (1984).
[3] J. Bijnens, G. Colangelo, G. Ecker, J. Gasser, and M. E. Sainio, Phys. Lett. B **374**, 210 (1996).
[4] J. Bijnens, G. Colangelo, G. Ecker, J. Gasser, and M. E. Sainio, Nucl. Phys. **B508**, 263 (1997); **B517**, 639(E) (1998).
[5] S. M. Roy, Phys. Lett. **B36**, 353 (1971).
[6] J. L. Basdevant, C. D. Froggatt, and J. L. Petersen, Nucl. Phys. **B72**, 413 (1974).

[7] B. Ananthanarayan, G. Colangelo, J. Gasser, and H. Leutwyler, Phys. Rep. **353**, 207 (2001).
[8] G. Colangelo, J. Gasser, and H. Leutwyler, Nucl. Phys. **B603**, 125 (2001).
[9] R. Garcia-Martin, R. Kaminski, J. R. Pelaez, J. Ruiz de Elvira, and F. J. Yndurain, Phys. Rev. D **83**, 074004 (2011).
[10] H. Leutwyler, arXiv:hep-ph/0612112.
[11] S. R. Beane, P. F. Bedaque, K. Orginos, and M. J. Savage, Phys. Rev. D **73**, 054503 (2006).
[12] S. R. Beane, T. C. Luu, K. Orginos, A. Parreno, M. J. Savage, A. Torok, and A. Walker-Loud, Phys. Rev. D **77**, 014505 (2008).
[13] X. Feng, K. Jansen, and D. B. Renner, Phys. Lett. B **684**, 268 (2010).
[14] T. Yamazaki *et al.* (CP-PACS Collaboration), Nucl. Phys. B, Proc. Suppl. **129**, 191 (2004).
[15] T. Yamazaki *et al.* (CP-PACS Collaboration), Phys. Rev. D **70**, 074513 (2004).
[16] S. Aoki *et al.* (CP-PACS Collaboration), Nucl. Phys. B, Proc. Suppl. **140**, 305 (2005).
[17] S. Aoki *et al.* (CP-PACS Collaboration), Phys. Rev. D **71**, 094504 (2005).
[18] J. J. Dudek, R. G. Edwards, M. J. Peardon, D. G. Richards, and C. E. Thomas, Phys. Rev. D **83**, 071504 (2011).
[19] S. R. Beane *et al.*, Phys. Rev. D **79**, 114502 (2009).
[20] S. R. Beane *et al.*, Phys. Rev. D **80**, 074501 (2009).
[21] S. R. Beane *et al.* (NPLQCD Collaboration), Phys. Rev. D **81**, 054505 (2010).
[22] S. R. Beane *et al.*, Phys. Rev. D **84**, 014507 (2011); **84**, 039903(E) (2011
[23] S. R. Beane *et al.* (NPLQCD Collaboration), Phys. Rev. Lett. **106**, 162001 (2011).
[24] L. Maiani and M. Testa, Phys. Lett. B **245**, 585 (1990).
[25] K. Huang and C. N. Yang, Phys. Rev. **105**, 767 (1957).
[26] H. W. Hamber, E. Marinari, G. Parisi, and C. Rebbi, Nucl. Phys. **B225**, 475 (1983).
[27] M. Lüscher, Commun. Math. Phys. **105**, 153 (1986).
[28] M. Lüscher, Nucl. Phys. **B354**, 531 (1991).
[29] S. R. Beane, P. F. Bedaque, A. Parreño, and M. J. Savage, Phys. Lett. B **585**, 106 (2004).
[30] K. Rummukainen and S. A. Gottlieb, Nucl. Phys. **B450**, 397 (1995).
[31] C. h. Kim, C. T. Sachrajda, and S. R. Sharpe, Nucl. Phys. **B727**, 218 (2005).
[32] N. H. Christ, C. Kim, and T. Yamazaki, Phys. Rev. D **72**, 114506 (2005).
[33] X. Feng *et al.* (ETM Collaboration), Proc. Sci., LAT2010 (2010) 104 [arXiv:1104.0058].
[34] C. B. Lang, D. Mohler, S. Prelovsek, and M. Vidmar, Phys. Rev. D **84**, 054503 (2011).
[35] J. J. Dudek, R. G. Edwards, M. J. Peardon, D. G. Richards, and C. E. Thomas, Phys. Rev. Lett. **103**, 262001 (2009).
[36] J. M. Bulava *et al.*, Phys. Rev. D **79**, 034505 (2009).
[37] H. W. Lin *et al.* (Hadron Spectrum Collaboration), Phys. Rev. D **79**, 034502 (2009).
[38] R. G. Edwards, B. Joo, and H. W. Lin, Phys. Rev. D **78**, 054501 (2008).
[39] M. Okamoto *et al.* (CP-PACS Collaboration), Phys. Rev. D **65**, 094508 (2002).
[40] P. Chen, Phys. Rev. D **64**, 034509 (2001).
[41] C. Morningstar and M. J. Peardon, Phys. Rev. D **69**, 054501 (2004).
[42] P. F. Bedaque, I. Sato, and A. Walker-Loud, Phys. Rev. D **73**, 074501 (2006).
[43] S. R. Beane *et al.* (NPLQCD Collaboration) arXiv:1108.1380.
[44] M. I. Buchoff, Phys. Rev. D **77**, 114502 (2008).
[45] W. Hoogland *et al.*, Nucl. Phys. **B126**, 109 (1977).
[46] D. H. Cohen, T. Ferbel, P. Slattery, and B. Werner, Phys. Rev. D **7**, 661 (1973).
[47] N. B. Durusoy, M. Baubillier, R. George, M. Goldberg, A. M. Touchard, N. Armenise, M. T. Fogli Muciaccia, and A. Silvestri, Phys. Lett. **45B**, 517 (1973).
[48] M. J. Losty *et al.*, Nucl. Phys. **B69**, 185 (1974).
[49] R. G. Edwards and B. Joo (SciDAC Collaboration), Nucl. Phys. B, Proc. Suppl.**140**, 832 (2005).